JACS
JOURNAL OF THE AMERICAN CHEMICAL SOCIETY

Article

pubs.acs.org/JACS

Chemoselective, Stereospecific, and Living Polymerization of Polar Divinyl Monomers by Chiral Zirconocenium Catalysts

Fernando Vidal, Ravikumar R. Gowda, and Eugene Y.-X. Chen*

Department of Chemistry, Colorado State University, Fort Collins, Colorado 80523-1872, United States

Supporting Information

ABSTRACT: This contribution reports the first chemoselective, stereospecific, and living polymerization of polar divinyl monomers, enabled by chiral *ansa*-zirconocenium catalysts through an enantiomorphic-site controlled coordination−addition polymerization mechanism. Silyl-bridged-*ansa*-zirconocenium ester enolate **2** has been synthesized and structurally characterized, but it exhibits low to negligible activity and stereospecificity in the polymerization of polar divinyl monomers including vinyl methacrylate (VMA), allyl methacrylate (AMA), 4-vinylbenzyl methacrylate (VBMA), and *N*,*N*-diallyl acrylamide (DAA). In contrast, ethylene-bridged-*ansa*-zirconocenium ester enolate **1** is highly active and stereospecific in the polymerization of such monomers including AMA, VBMA, and DAA. The polymerization by **1** is perfectly chemoselective for all four polar divinyl monomers, proceeding exclusively through conjugate addition across the methacrylic C═C bond, while leaving the pendant C═C bonds intact. The polymerization of DAA is most stereospecific and controlled, producing essentially stereoperfect isotactic PDAA with [*mmmm*] > 99%, M_n matching the theoretical value (thus a quantitative initiation efficiency), and a narrow molecular weight distribution ($Đ$ = 1.06−1.16). The stereospecificity is slightly lower for the AMA polymerization but still leading to highly isotactic poly(allyl methacrylate) (PAMA) with 95−97% [*mm*]. The polymerization of VBMA is further less stereospecific, affording PVBMA with 90−94% [*mm*], while the polymerization VMA is least stereospecific. Several lines of evidence from both homo- and block copolymerization results have demonstrated living characteristics of the AMA polymerization by **1**. Mechanistic studies of this polymerization have yielded a monometallic coordination−addition polymerization mechanism involving the eight-membered chelating intermediate. Post-functionalization of isotactic polymers bearing the pendant vinyl group on every repeating unit via the thiol−ene "click" reaction achieves a full conversion of all the pendant double bonds to the corresponding thioether bonds. Photocuring of such isotactic polymers is also successful, producing an elastic material readily characterizable by dynamic mechanical analysis.

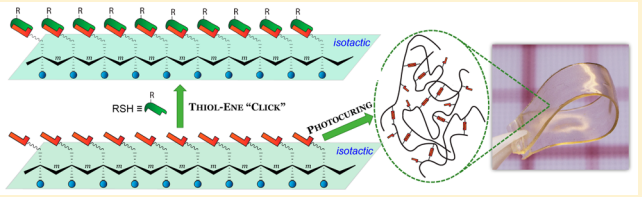

INTRODUCTION

Since the discovery of Ziegler−Natta polymerization, metal-mediated coordination polymerization has evolved into arguably the most powerful technique for controlling the polymerization stereochemistry.[1] In the polymerization of vinyl monomers, the metal-mediated coordination polymerization can be categorized into coordination−insertion and coordination−addition polymerizations. The coordination−insertion polymerization is typically catalytic in both fundamental monomer enchainment and polymer chain production and is applied to nonpolar olefins as well as copolymerization of nonpolar and polar olefins.[2] In comparison, the coordination−addition polymerization concerns conjugated polar olefins such as acrylics and is commonly living or quasi-living, thus noncatalytic in polymer chain production,[3] although the catalytic coordination−addition polymerization of acrylics has recently been established by zirconocenium-hydridoborate ion pairs via a hydride-shuttling chain-transfer mechanism.[4]

Polymers bearing active vinyl groups attached to the main chain can be readily post-functionalized through the retaining vinyl groups to a variety of useful functional materials.[5] However, polymerization of divinyl monomers with complete chemoselectivity by safeguarding one of the reactive vinyl groups while selectively polymerizing the other has been a challenging task. Vinyl methacrylates, such as allyl methacrylate (AMA) that exhibits a large reactivity difference (r_1/r_2 = 30) between the conjugated (r_1 = 1.8) and nonconjugated (r_2 = 0.06) vinyl groups, appear to be good candidates for achieving complete chemoselective polymerization, but its radical polymerization[6] still cannot maintain the chemoselectivity throughout the entire reaction process, especially in the later stage of the polymerization when additions to the pendant nonconjugated double bonds also occur, resulting in gelation due to formation of cross-linked network structures.[7] The radical polymerization of vinyl methacrylate (VMA, r_1 = 18, r_2 = 0.011) in the presence of a suitable aluminum Lewis acid achieved the chemoselectivity up to 85% monomer conversion to produce a soluble polymer,[8] and anionic polymerization of VMA showed high chemoselectivity.[9] For polar divinyl monomers with a similar reactivity for both vinyl groups such as 4-vinylbenzyl methacrylate (VBMA; r_1 = 1.04 for the

Received: June 4, 2015
Published: July 8, 2015

DOI: 10.1021/jacs.5b05811
J. Am. Chem. Soc. 2015, 137, 9469−9480

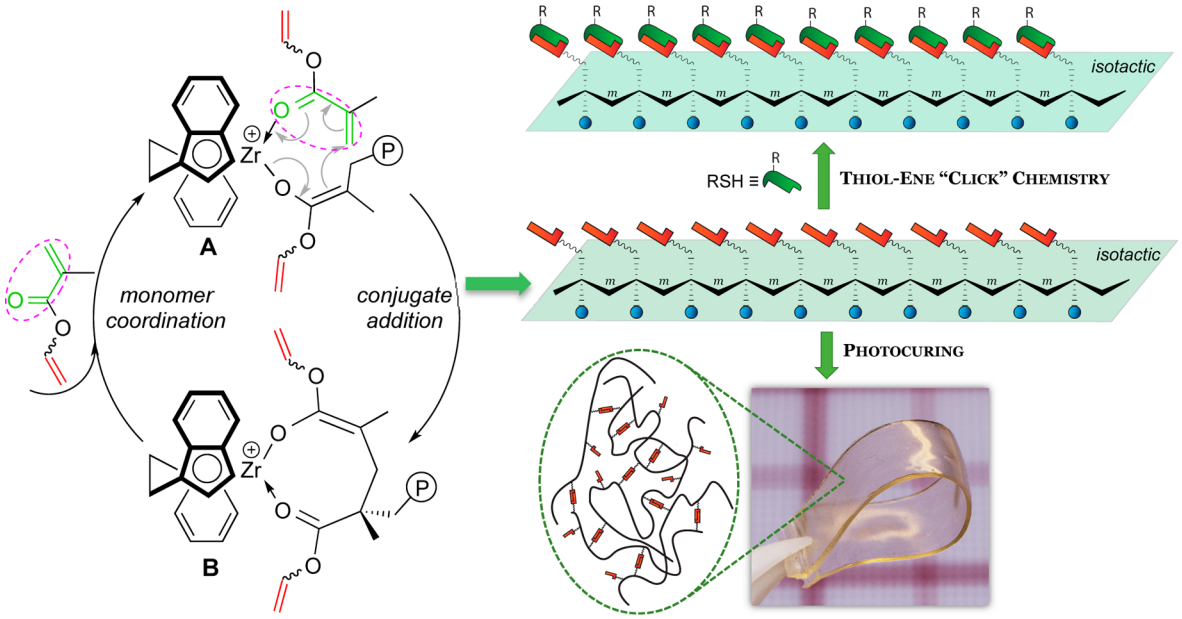

Figure 1. Schematic representation of the hypothesis for isotactic acrylic polymers carrying pendant vinyl groups to be synthesized by stereospecific coordination–addition polymerization of polar divinyl monomers with chiral zirconocenium catalysts and subsequently post-functionalized via the thiol–ene "click" reaction and photocuring to advanced functional materials.

Scheme 1. Synthetic Route to *rac*-(SBBI)Zr$^+$(THF)[OC(O^{i}Pr)=CMe$_2$][MeB(C$_6$F$_5$)$_3$]$^-$ (2)

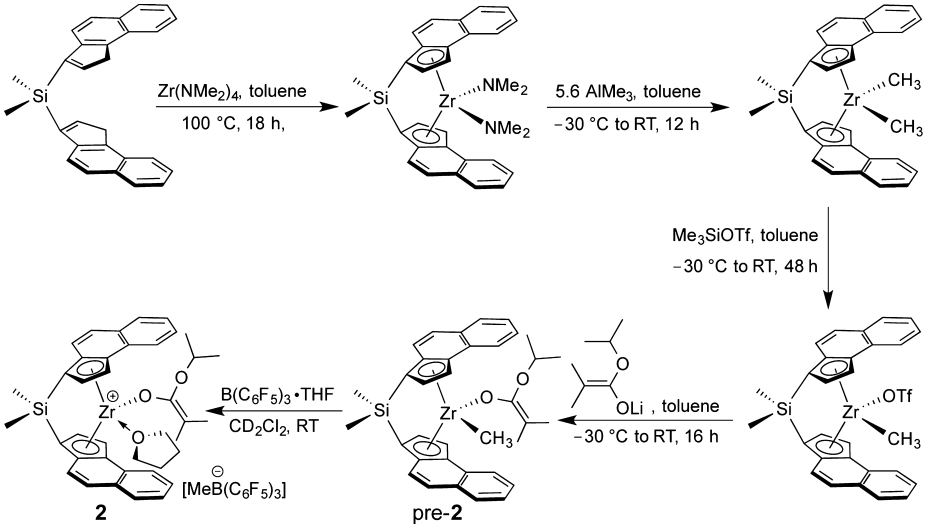

methacrylic C=C bond and r_2 = 0.85 for the styrenic C=C bond), their radical polymerizations can lead to gelation even at the early stage of the reaction.[10] Group transfer polymerization of VBMA yielded PVBMA with a broad molecular weight distribution ($Đ$) of 8.2, due to polymerization of some styrenic double bonds as well.[11] Anionic polymerization of VBMA by resonance-stabilized initiators such as 1,1-diphenylhexyl lithium and trityl potassium was controlled and selective toward polymerizing the polar double bonds at −78 °C, but such desired characteristics were lost when the reaction was carried out at higher temperatures (−20 °C or above).[12] Most recently, the complete chemoselective polymerization of AMA, VBMA, and VMA has been achieved at room temperature (RT) utilizing the Lewis pair (LP) cooperativity in the LP polymerization[13] by *N*-heterocyclic carbene (NHC) and *N*-heterocyclic carbene olefin (NHO) based LPs consisting of NHC/B(C$_6$F$_5$)$_3$,[14] and NHC or NHO/Al(C$_6$F$_5$)$_3$,[10] producing uncross-linked, soluble functional polymers with $Đ$ < 1.6.

Ideally, polymerization of such polar divinyl monomers should be not only chemoselective, but also stereospecific and living, thus offering an opportunity to synthesize advanced functional polymeric materials with both well-controlled chain structures and stereochemistry, two essential features affecting the physical and mechanical properties of the polymers. To meet this challenge, we hypothesized that chiral *ansa*-zirconocenium ester enolate complexes, which are known to polymerize alkyl methacrylates[15,16] and acrylamides[17] in a stereospecific and living fashion, should be chemoselective, stereospecific, and living in polymerization of polar divinyl monomers, due to their catalyst site-controlled coordination–addition mechanism that should involve exclusive conjugate addition across the methacrylic double bond that is most activated via coordination of the conjugated carbonyl to the

DOI: 10.1021/jacs.5b05811
J. Am. Chem. Soc. 2015, 137, 9469–9480

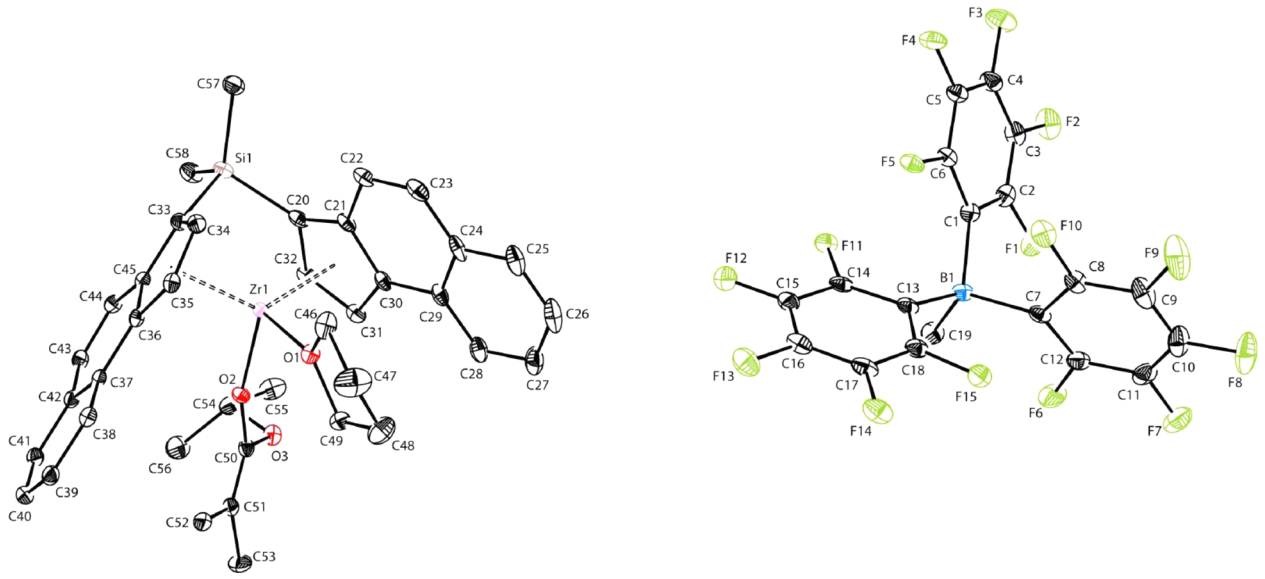

Figure 2. X-ray crystal structure of *rac*-(SBBI)Zr^{+}(THF)[OC(O^{i}Pr)=CMe_2][$MeB(C_6F_5)_3$]$^{-}$ (**2**) with thermal ellipsoids drawn at the 40% probability. Selected bond lengths (Å) and angles (deg): Zr(1)−O(1) 2.202(16), Zr(1)−O(2) 1.943(15), Zr(1)−Cp(1) 2.537(av.), Zr(1)−Cp(2) 2.552(av.), C(50)−C(51) 1.332(3), B(1)−C(1) 1.675(4), B(1)−C(7) 1.650(4), B(1)−C(13) 1.659(4), B(1)−C(19) 1.641(4); O(2)−Zr(1)−O(1) 92.69(6), C(1)−B(1)−C(7) 103.4(2), C(1)−B(1)−C(13) 113.1(2), C(7)−B(1)−C(13) 113.1(2).

cationic Zr center, thus leaving the pendant C=C bonds intact (Figure 1). Such well-defined polymers could be post-functionalized via the thiol−ene "click" reaction[18] and/or photocuring to advanced functional materials.

RESULTS AND DISCUSSION

Synthesis and Structure of *rac*-(SBBI)Zr^{+}(THF)[OC(O^{i}Pr)=CMe_2][$MeB(C_6F_5)_3$]$^{-}$ (2). Chiral ethylene-bridged-bis(indenyl)-*ansa*-zirconocenium ester enolate *rac*-(EBI)-Zr^{+}(THF)[OC(O^{i}Pr)=CMe_2] [$MeB(C_6F_5)_3$]$^{-}$ [**1**, EBI = ethylene-bis(η^5-indenyl)][15] has been a workhorse catalyst for stereospecific and living coordination−addition polymerization of polar conjugated alkenes or α,β-unsaturated esters and amides (acrylic monomers), which enabled the synthesis of highly isotactic poly(methacrylate)s,[15,16] poly(acrylamide)s,[17] and poly(β-methyl-α-methylene-γ-butyrolactone)[19] as well as optically active helical poly(*N*,*N*-diarylacrylamide)s.[20] In the case of the coordination−insertion polymerization of propylene, it has been shown that catalysts based on silyl-bridged-bis(substituted indenyl)-*ansa*-zircononcenes are superior to those ethylene-bridged analogues in both activity and stereospecificity.[21] Interestingly, for coordination−addition polymerization of methyl methacrylate (MMA), an opposite trend was observed, with the ethylene-bridged-bis(indenyl)-based catalyst producing poly(methyl methacrylate) (PMMA) having a higher isotacticity (96% *mm*) than that (90% *mm*) produced by the silyl-bridged-bis(indenyl)-based catalyst.[22] Hence, we were interested in examining if substituents on the indenyl rings could render a chiral silyl-bridged-*ansa*-zircononcenium ester enolate catalyst to exhibit superior catalytic performance to the ethylene-bridged catalyst **1** in the coordination−addition polymerization of polar divinyl monomers.

Using the general procedure previously established for the synthesis of **1**,[15,16,23] Scheme 1 outlines the synthetic route to the new chiral, silyl-bridged-*ansa*-zirconocene ester enolate *rac*-(SBBI)Zr^{+}(THF) [OC(O^{i}Pr)=CMe_2][$MeB(C_6F_5)_3$]$^{-}$ [**2**, SBBI = (dimethyl)silyl-bis(benz[*e*]-η^5-indenyl)]. Starting from the neutral ligand bis[3,3′-(3-*H*-benz[*e*]indenyl)]dimethylsilane,[21a] the corresponding C_2-chiral zirconocene amide complex, *rac*-(SBBI)$Zr(NMe_2)_2$, was prepared as orange crystals in 68% yield, using the modified procedure for the stereoselective amine-elimination approach to the ethylene-bis(indenyl) derivative, *rac*-(EBI)$Zr(NMe_2)_2$.[24] Next, alkylation of the amide complex with excess $AlMe_3$ led to the corresponding dimethyl complex *rac*-(SBBI)$ZrMe_2$. Treatment of the dimethyl derivative with Me_3SiOTf afforded the methyl triflate complex *rac*-(SBBI)ZrMe(OTf) as orange crystals, which was subsequently reacted with Me_2C=C(O^{i}Pr)OLi to form the methyl ester enolate precatalyst, *rac*-(SBBI)ZrMe-[OC(O^{i}Pr)=CMe_2] (pre-**2**) in 86% yield (Figure S6). In the final step, the cationic ester enolate **2** was cleanly and quantitatively generated by *in situ* mixing of pre-**2** with $(C_6F_5)_3B$·THF in CD_2Cl_2 at RT (Figure S7), following the procedure established for generation of cation **1**.[15,16] After methide abstraction by the borane, the methyl group downfield-shifted drastically in ^{1}H NMR from δ −0.78 ppm (C_7D_8) when attached to Zr in pre-**2** to δ 0.48 ppm (CD_2Cl_2) now attached to B of the anion [$MeB(C_6F_5)_3$]$^{-}$ in **2**; this chemical shift is identical to that observed in cation **1**[15] and nearly identical to that reported for the unassociated, free [$MeB(C_6F_5)_3$]$^{-}$ anion (δ 0.51 ppm in CD_2Cl_2).[25] The noncoordinating nature of the anion [$MeB(C_6F_5)_3$]$^{-}$ in **2** is also established by the ^{19}F NMR spectrum in which a small chemical shift difference of <3 ppm between the *para*- and *meta*-fluorines is diagnostic of the noncoordinating [MeB-$(C_6F_5)_3$]$^{-}$ anion[25,26] [$\Delta(m,p$-F) = 2.6 ppm in **2**].

Single crystal X-ray diffraction analysis confirmed the molecular structure of **2** as depicted in Scheme 1, featuring the unassociated ion pair consisting of the THF-stabilized zirconocene ester enolate cation and the methyl borate anion (Figure 2). The coordinated THF is datively bonded to Zr with a Zr(1)−O(1) distance of 2.202(16) Å, whereas the ester enolate ligand is covalently bonded to Zr with a Zr(1)−O(2) distance of 1.943(15) Å. The C(50)=C(51) double bond in the ester enolate moiety is characterized by a bond distance of 1.332(3) Å and sums of the angles 359.9° and 360.0° around

DOI: 10.1021/jacs.5b05811
J. Am. Chem. Soc. 2015, 137, 9469−9480

C(50) and C(51), respectively, for sp^2-hybridized C(50) and C(51) with a trigonal-planar geometry. The average B−C(aryl) distance (1.661 Å) is identical to that observed in the noncoordinating $[MeB(C_6F_5)_3]^-$ anion,[25] but the B−C(methyl) distance [1.641(4) Å] is slightly shorter than that [1.663(5) Å] reported for the $[MeB(C_6F_5)_3]^-$ anion that is still coordinated to the cationic Zr center.[27]

Polymerization Characteristics of Polar Divinyl Monomers by Chiral Zirconocene Catalysts. Previous reports from our group have shown that the polymerization of acrylic monomers such as alkyl methacrylates and *N*,*N*-dialkyl or diaryl acrylamides by cationic, C_2-ligated chiral *ansa*-zirconocene complexes such as **1** is isospecific and living, which proceeds through a monometallic, catalyst-site-controlled coordination−addition polymerization mechanism via eight-membered-ring ester or amide enolate intermediates.[15−17,19,20] In this work, we utilized such isospecific catalysts to polymerize acrylic monomers carrying a pendant C=C double bond, including VMA, AMA, VBMA, and *N*,*N*-diallyl acrylamide (DAA), aiming to achieve the chemoselective, stereospecific, and living polymerization of such monomers (Figure 3).

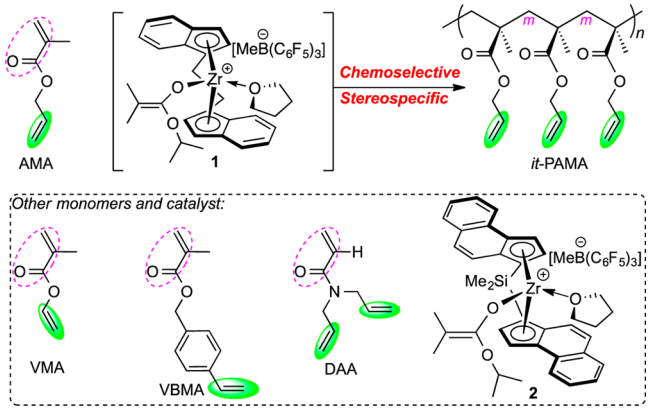

Figure 3. Chemoselective and stereospecific polymerization of polar divinyl monomers and structures of monomers, catalysts, and polymers (only one example shown).

Selected results for the polymerization of the four representative polar divinyl monomers by catalyst **1**, which is generated by *in situ* mixing of *rac*-(EBI)ZrMe[OC(O^{i}Pr)=CMe$_2$] (pre-**1**) and $(C_6F_5)_3B{\cdot}THF$ in CH_2Cl_2 or toluene at RT,[15,16] are summarized in Table 1. First, control experiments were performed by mixing each monomer (200 equiv) with the pre-**1** and the activator $(C_6F_5)_3B{\cdot}THF$ individually in CH_2Cl_2, followed by stirring each mixture at RT for 24 h. No monomer conversion or gel formation was detected from those control runs, indicating that neither the neutral precatalyst nor the activator itself can promote the polymerization. Second, initial polymerization scanning revealed that the cationic **2** exhibited low stereospecificity even for the parent monomer MMA and low to negligible activity for polymerization of the current polar divinyl monomers (Table S1). Hence, the subsequent polymerization studies focused exclusively on catalyst **1**.

Next, we examined the polymerization of VMA in [VMA]/[**1**] ratios ranging 100−400 or with 1.0−0.25 mol % catalyst loadings (runs 1−3, Table 1). These reactions were homogeneous in CH_2Cl_2 and proceeded to high conversions (>99%) without signs of gel formation. The polymerizations were rapid, achieving quantitative or near quantitative conversion in short times (5−15 min). The number-average molecular weight (M_n) of the resulting PVMA increased from 20.6 kg/mol to 35.7 kg/mol to 64.0 kg/mol with an increase in the [VMA]/[**1**] ratio from 100 to 200 to 400, respectively, while the molecular weight distribution remained relatively narrow ($Đ$ = 1.18−1.29, Figure 4), showing some characteristics of a living polymerization. The PVMA materials produced by **1** are completely soluble in common organic solvents such as $CHCl_3$, toluene, and DMF, showing no signs of cross-linking. The materials exhibited a glass-transition temperature (T_g) between 44 and 49 °C and showed an onset decomposition temperature (T_d) of 279 °C and a two-step decomposition window accompanied by two maximum rate decomposition temperatures (T_{max}) of 324 and 411 °C (Figure S2). Significantly, ^{1}H NMR spectrum of the isolated PVMA revealed complete disappearance of the methacrylic =CH$_2$ proton signals at δ 6.23 and 5.68 ppm and complete retention of the pendant vinyl group −CH=CH$_2$ proton signals centered at δ 4.88, 4.60, and 7.14 ppm (Figure S13), indicating

Table 1. Selected Results of Polymerization of Polar Divinyl Monomers by Catalyst 1[a]

run no.	M	[M]/[1]	solvent	time (min)	conv.[b] (%)	M_n[c] (kg/mol)	$Đ$[c] (M_w/M_n)	[*mm*][d] (%)	[*mr*][d] (%)	[*rr*][d] (%)	T_g[e] (°C)
1	VMA	100	DCM	5	99	20.6	1.18	50.9	29.6	19.5	44.5
2	VMA	200	DCM	10	99	35.7	1.18	51.4	28.8	19.8	44.2
3	VMA	400	DCM	15	97	64.0	1.29	52.8	28.0	19.2	49.0
4	AMA	48	Tol	5	97	8.50	1.19	95.6	2.9	1.5	−13.0
5	AMA	97	Tol	7	95	15.5	1.18	95.5	3.0	1.5	−5.7
6	AMA	193	Tol	15	93	33.2	1.19	95.8	2.8	1.4	−2.7
7	AMA	300	Tol	45	97	43.8	1.18	97.0	2.0	1.0	−0.3
8	AMA	400	Tol	90	96	59.8	1.25	96.3	2.5	1.2	0.0
9	VBMA	100	DCM	15	75	15.3	1.18	90.0	6.4	3.6	44.5
10	VBMA	100	DCM	30	95	31.3	2.94	90.0	6.9	3.1	48.2
11	VBMA	100	Tol	30	99	27.1	3.03	93.6	4.3	2.1	57.0
12	VBMA	200	Tol	60	75	30.0	1.42	92.8	4.8	2.4	61.0
13	DAA	101	DCM	30	99	18.3	1.06	>99	–	–	–
14	DAA	202	DCM	120	97	30.2	1.16	>99	–	–	–

[a]Conditions: solvent (DCM = CH_2Cl_2 or Tol = toluene) = 5 mL; ambient temperature (~23 °C). n.d. = not determined. [b]Monomer (M) conversion measured by ^{1}H NMR. [c]Number-average molecular weight (M_n) and polydispersity ($Đ$) determined by gel-permeation chromatography (GPC) relative to PMMA standards. [d]Tacticity measured by ^{1}H or ^{13}C NMR in $CDCl_3$. [e]Glass-transition temperature (T_g) measured by DSC.

DOI: 10.1021/jacs.5b05811
J. Am. Chem. Soc. 2015, 137, 9469−9480

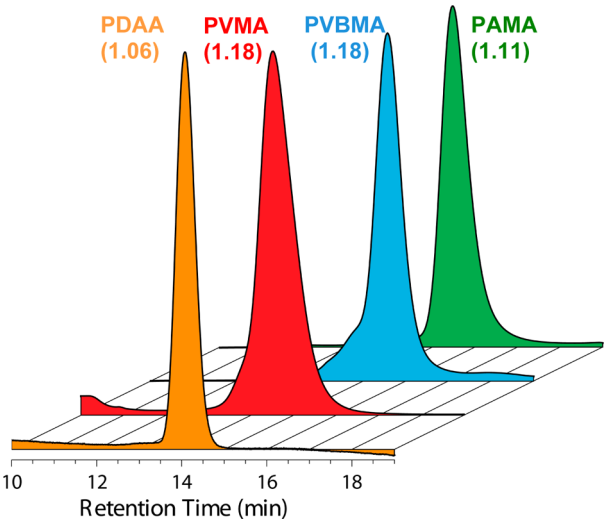

Figure 4. Representative GPC traces of the polymers produced and associated $Đ$ values.

that the polymerization proceeded exclusively through conjugate addition across the methacrylic double bond. However, the PVMA produced is only an isotactic-biased material, with [*mm*] = 51−53%. In comparison, polymerization of alkyl methacrylates such as *n*-butyl methacrylate by catalyst **1** produces highly isotactic polymer with [*mm*] up to 99%.[15] In short, the coordination−addition polymerization of VMA by catalyst **1** is controlled and chemoselective, but it lacks high stereospecificity thus producing only iso-biased PVMA.

In sharp contrast, the polymerization of AMA by catalyst **1** is not only controlled and completely chemoselective but also highly stereospecific. Thus, varying the [AMA]/[**1**] ratio from 48 to 400 (runs 4−8, Table 1), the polymerization in toluene achieved high conversions and produced the corresponding poly(allyl methacrylate) (PAMA) with gradually increased M_n from 8.5 kg/mol to 59.8 kg/mol, while the $Đ$ remained narrow (from 1.11 to 1.25, Figure 4). The initiation efficiency [I^* = M_n(calcd)/M_n(exptl), where M_n(calcd) = MW(M) × [M]/[**1**] × conv (%) + MW of chain-end groups] of this polymerization was relatively high (71−84%). The isolated PAMA is soluble in common organic solvents and exhibited a T_g ranging from −13 to 0 °C which gradually increased as M_n increased (runs 4−8, Table 1). This polymer is rather stable if stored at RT in dark, but cross-linking occurred within 24 h of exposure to ambient laboratory light conditions, after which addition of $CHCl_3$ to the sample revealed the formation of insoluble cross-linked fractions. Hence, the samples of this polymer were stored in brown bottles at −20 °C to preserve the integrity of the polymer for further functionalization studies (*vide infra*). Polymerizations carried out in CH_2Cl_2 yielded PAMA materials with similar characteristics to those produced in toluene, but the activity was lower.

The chemoselectivity of the AMA polymerization by **1** is perfect, as evidenced by the complete retention of the vinyl groups (δ 5.91, 5.31, and 5.20 ppm in ^{1}H NMR, Figure 5). Significantly, the AMA polymerization is also highly stereospecific, producing *it*-PAMA with a high isotacticity of [*mm*] = 95−97% (Figure 5) and 2[*rr*]/[*mr*] = 1, indicative of the enantiomorphic-site controlled mechanism. Furthermore, the ^{13}C NMR spectrum of the polymer provided corroborated evidence for the formation of the highly isotactic *it*-PAMA (Figure 6). It is intriguing that the placement of the sp^3-hybridized (bulkier) CH_2 group between the ester oxygen atom and the sp^2-hybridized (less bulky) vinyl moiety in the case of AMA had such a profound effect on the polymerization stereospecificity (relative to VMA without the CH_2 group), highlighting the importance of the sterics and orientation of the ester OR group of the methacrylate monomer in the transition-state structure that determines the stereospecificity of the metallocene-catalyzed polymerization.[28]

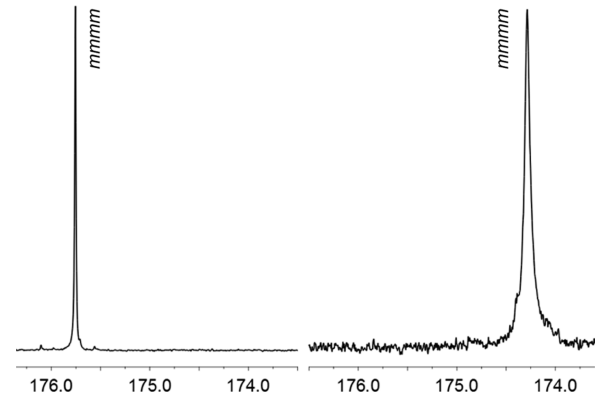

Figure 6. ^{13}C NMR spectra ($CDCl_3$, 50 °C) showing the C═O pentad (*mmmm*) region of the highly isotactic PAMA (left) and highly isotactic PDAA (right).

Chemoselective polymerization of VBMA is especially challenging for free radical or anionic polymerization, due to similar reactivity ratios between the methacrylic C═C bond (r_1

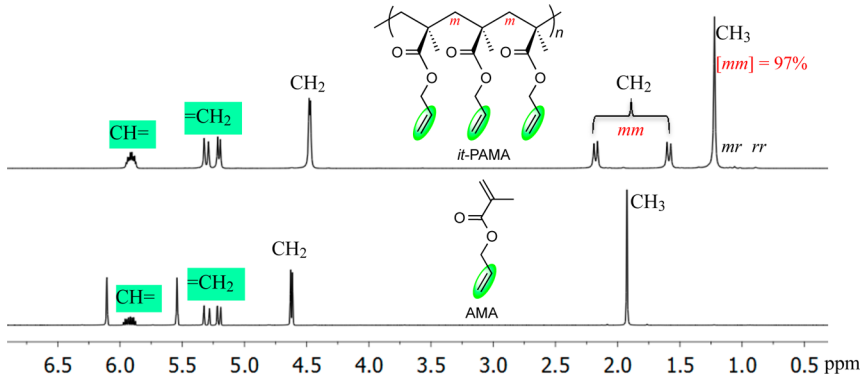

Figure 5. Overlay of ^{1}H NMR ($CDCl_3$, 25 °C) spectra of the monomer AMA and polymer *it*-PAMA.

DOI: 10.1021/jacs.5b05811
J. Am. Chem. Soc. 2015, 137, 9469−9480

= 1.04) and styrenic C═C bond (r_2 = 0.84).[29] However, the metallocene-catalyzed coordination−addition polymerization readily promotes the chemoselective polymerization of VBMA. For example, the VBMA polymerization in a [VBMA]/[**1**] ratio of 100 in CH_2Cl_2 (runs 9−10) and toluene (run 11, Table 1) achieved high (95%) to almost quantitative (99%) conversion while maintaining a homogeneous solution with no gelation or precipitation to yield completely soluble polymers. Subsequent analysis of the isolated material by ^{1}H NMR showed that the methacrylate vinyl protons (δ 5.57 and 6.14 ppm) completely disappeared while the vinylbenzyl moiety (δ 5.18, 5.65, and 6.61 ppm) was left intact (Figure S16). Note that the integration for the signals corresponding to the vinylbenzyl group matched with those of the main-chain aliphatic backbone, implying the vinylbenzyl moiety was retained in every repeating unit. Although the PVBMA obtained at 75% conversion had a narrow polydispersity $Đ$ = 1.18 (Figure 4) and a quantitative I* of 100% (run 9), the PVBMA produced at near quantitative conversions of 95% or 99% started to show much higher $Đ$ values of ∼3, indicating possible polymerization of the styrenic moiety by the cationic catalyst after the complete or nearly complete conversion of the methacrylic C═C bond. In addition, thermal cross-linking of the isolated PVBMA can be observed even in the solid state when stored at RT. Indeed, analysis of PVBMA by differential scanning calorimetry (DSC) showed a thermal cross-linking exothermic peak with an onset temperature and a peak maximum of 119 and 164 °C, respectively. Importantly, the resulting PVBMA is isotactic, with [*mm*] = 90.0%−93.6%. A test of the polymer stereoerrors gave 2[*rr*]/[*mr*] = 1, confirming the same enantiomorphic-site controlled mechanism as that described for AMA polymerization.

The chemoselectivity and stereospecificity of catalyst **1** toward polymerization of polar divinyl monomers is further demonstrated by investigation into the polymerization characteristics of the acrylamide monomer DAA. Specifically, the polymerization with a [DAA]/[**1**] ratio of 101 in CH_2Cl_2 achieved 99% conversion in 30 min (run 13), producing the corresponding soluble poly(*N*,*N*-diallyl acrylamide) (PDAA) with M_n = 18.3 and $Đ$ = 1.06 (Figure 4). The run at a higher [DAA]/[**1**] ratio of 202 in CH_2Cl_2 proceeded in a similar controlled fashion, affording PDAA with M_n = 30.2 and $Đ$ = 1.16 as well as a quantitative I* value of 99% (run 14). Although the activity of the DAA polymerization is the slowest of the series, quantitative or near quantitative DAA conversion can be achieved in all the tested ratios without any sign of polymer cross-linking or degradation in solution. PDAA showed a high T_d of 445 °C and a single decomposition window with a high T_{max} of 469 °C (Figure S5). Importantly, the quantitative chemoselectivity and stereospecificity of this polymerization were confirmed by the analysis of the ^{1}H (Figure S12) and ^{13}C NMR (Figure 6) spectra of the isolated material.

Livingness, Kinetics, and Mechanism of Polymerization. Three lines of key evidence, summarized below using the AMA polymerization by **1** as an example, clearly showed living characteristics of this polymerization. First, the M_n of PAMA increased linearly (R^2 = 0.996) with an increase in the [AMA]/[**1**] ratio from 50 to 400 (Figure 7), while the $Đ$ remained narrow (from 1.11 to 1.25). Second, a plot of the polymer M_n vs monomer conversion at a fixed $[AMA]_0/[\mathbf{1}]_0$ ratio 300 also gave a straight line (R^2 = 0.995), which was coupled with the small $Đ$ values (Figure 8). Third, block

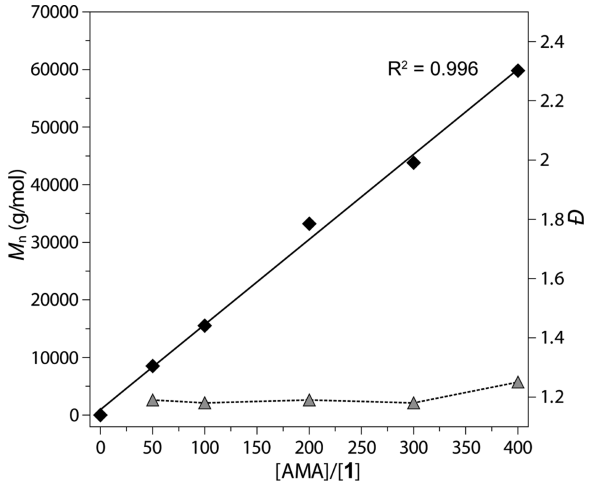

Figure 7. Plot of M_n and $Đ$ of *it*-PAMA produced by **1** vs $[AMA]_0/[\mathbf{1}]_0$ ratio (toluene, 23 °C).

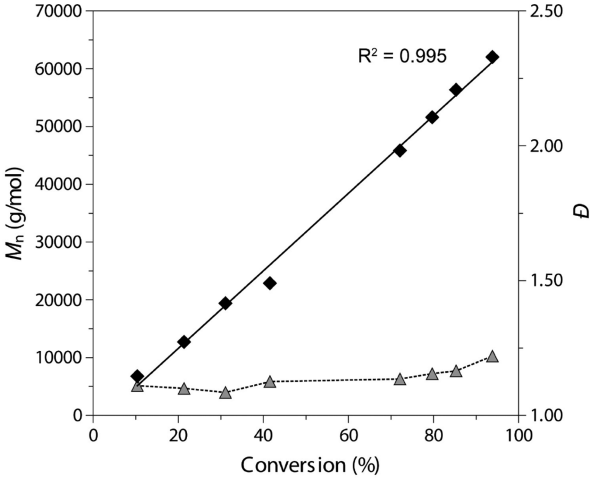

Figure 8. Plot of M_n and $Đ$ of *it*-PAMA produced by **1** vs monomer conversion with a $[AMA]_0/[\mathbf{1}]_0$ ratio of 300 (toluene, 23 °C).

copolymerizations by **1** allowed the synthesis of the well-defined block copolymers PMMA-*b*-PAMA and PMMA-*b*-PDAA with unimodal, narrow MW distributions ($Đ$ = 1.14−1.28). The block copolymerizations were started by polymerization of MMA (200 equiv, 100% conversion in 30 min), followed by AMA (200 equiv, 97% conversion, 60 min) or DAA (200 equiv, 99% conversion, 120 min) polymerization, producing in both cases well-defined block copolymers PMMA-*b*-PAMA ($Đ$ = 1.28) and PMMA-*b*-PDAA ($Đ$ = 1.14). The measured M_n's of the resulting PMMA-*b*-PAMA and PMMA-*b*-PDAA were 65.6 kg/mol and 69.8 kg/mol, respectively, corresponding to an I* value of ∼70% for both cases. As a quantitative or near quantitative conversion was achieved for both monomers in the block copolymerization, the molar composition of the block copolymers measured by ^{1}H NMR was the same as the molar feed ratio (1:1). Also as expected, two T_g's were observed for PMMA-*b*-PAMA, characteristic of each of the component segments: $T_g(1)$ = 56.6 °C for the *it*-PMMA block, $T_g(2)$ = 6.5 °C for the *it*-PAMA block. Both block copolymers are also highly isotactic, similar to their respective isotactic homopolymers. It is worth noting here that reversing the addition sequence of both block copolymerizations resulted in formation of either a block-/homopolymer

DOI: 10.1021/jacs.5b05811
J. Am. Chem. Soc. 2015, 137, 9469−9480

mixture or only a homopolymer, due to a change of the basicity and the coordination strength to the metal center of the incoming monomer relative to the last coordinated monomer unit in the chelating catalyst resting state (e.g., **B** in Figure 1), which determines whether the second monomer can ring-open the chelate to be polymerized or not, characteristic of the metallocene-mediated coordination−addition block copolymerization (i.e., monomers can only be copolymerized in order of increasing coordination strength).[3a,17]

Next, we examined the kinetics of AMA polymerization by catalyst **1**, revealing the polymerization is first order with respect to monomer concentration [AMA] for all the $[AMA]_0/[\mathbf{1}]_0$ ratios investigated (48−322, Figure 9). A double logarithm

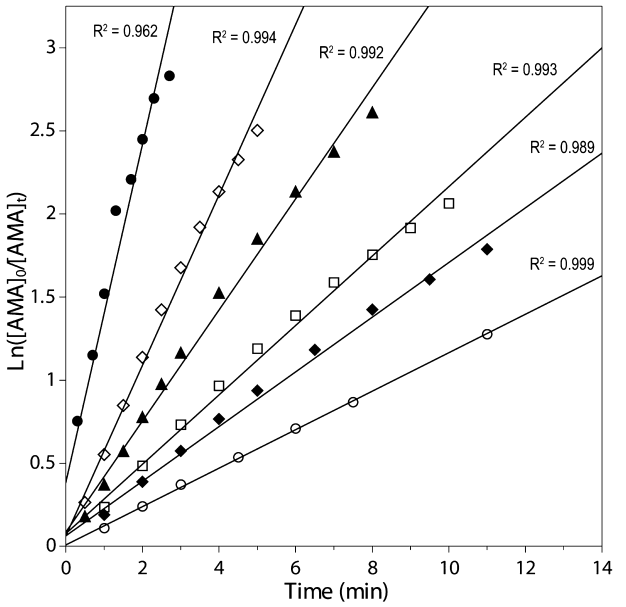

Figure 9. Semilogarithmic plots of $\ln\{[AMA]_0/[AMA]_t\}$ vs time for the polymerization of AMA by **1** in toluene at 23 °C. Conditions: $[AMA]_0$ = 0.697 M; $[\mathbf{1}]_0$ = 14.44 mM (●), 7.22 mM (◇), 5.41 mM (▲), 3.61 mM (□), 2.89 mM (◆), and 2.16 mM (○).

plot (Figure 10) of the apparent rate constants (k_{app}), obtained from the slopes of the best-fit lines to the plots of $\ln([AMA]_0/[AMA]_t)$ vs time, as a function of $\ln[\mathbf{1}]_0$, was fit to a straight line (R^2 = 0.995) with a slope of 1.1. Thus, the kinetic order with respect to [**1**], given by the slope of ∼1, reveals that the propagation is also first order in catalyst concentration. These results indicate that the resting state in the proposed monometallic propagation "catalysis" cycle (Scheme 2) is the cyclic ester enolate **B**, which was structurally modeled by the isolated cationic cyclic ester enolate complex **3** (*vide infra*) and that associative displacement of the coordinated ester group by incoming monomer to regenerate the active species **A** is the rate-determining step (i.e., **B** → **A**, Scheme 2). These key features of the mechanism are the same as those already shown for the coordination−addition polymerization of alkyl methacrylates.[15,16]

The above-proposed mechanism suggests the possibility to isolate the first-monomer-addition product **3** serving as the structural model of the resting intermediate **B**, since the monomer addition is fast relative to the monomer coordination in the propagation "catalysis" cycle depicted in Scheme 2. Accordingly, we carried out the stoichiometric reaction between the cationic ester enolate **1** (itself also a structural model for the

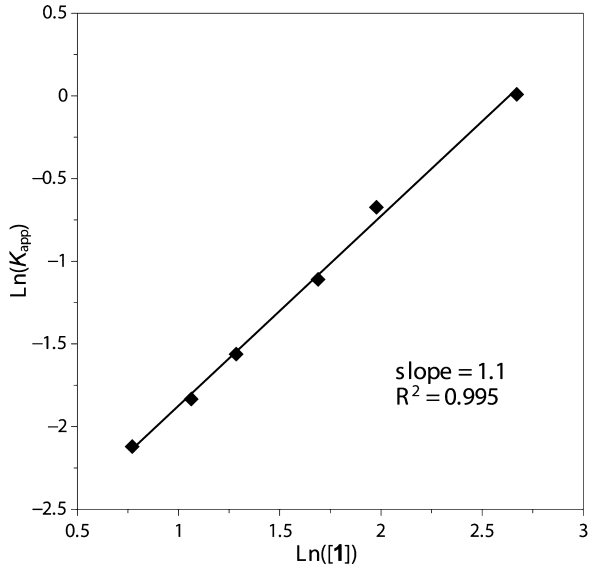

Figure 10. Plot of $\ln(k_{app})$ vs $\ln[\mathbf{1}]$ for the AMA polymerization by **1** in toluene at 23 °C.

active species **A**) and 1 equiv of AMA in CD_2Cl_2 at RT. Monitoring the reaction by ^{1}H NMR revealed rapid consumption of AMA upon its addition, but the signals corresponding to Zr species suggested coexistence of two separate species, **3** and **3**·THF (Figure S8). Signals characteristic of **3** are a septet at δ 4.34 ppm for $-OCHMe_2$ of the coordinated isopropyl ester group [$-C(O^iPr)=O$], a sharp singlet at δ 1.57 ppm for $=CMe$, and two doublets at δ 1.40 and 1.28 ppm for $-OCHMe_2$. The chemoselective Michael addition of AMA is confirmed by the observation of the fully intact allyl group in **3** with its characteristic signals at δ 5.87, 5.29, 5.23, and 3.83 ppm. However, the color of the mixture changed from bright red to orange upon standing at RT for several hours, indicating the spontaneous evolution of the reaction. Indeed, the ^{1}H NMR spectrum confirmed the formation of **3**·THF as the major product, which corresponds to the cleavage (opening) of the eight-membered chelate in **3** by the free THF present in the solution, as evidenced by the observations of: (a) the markedly downfield shifting of $-OCHMe_2$ from δ 4.36 in **3** to 4.96 ppm in **3**·THF for the noncoordinated isopropyl ester group; (b) the upfield shifting of signals corresponding to the coordinated THF molecule in **3**·THF (δ 3.66 and 3.52 ppm for α-CH_2, δ 1.87 ppm for β-CH_2, vs signals at δ 3.88 and 1.96 ppm for the free THF); and (c) the appearance of only one doublet for $-OCHMe_2$ of the noncoordinated isopropyl ester group, which was also upfield shifted from the coordinated analogue to δ 1.25 ppm.

Being isostructural to complex **1** and active species **A**, complex **3**·THF was isolated in the preparative scale as a bright yellow powder. The coordinated THF molecule was not removed even after extensive drying *in vacuo* for 8 h at RT or heating at 80 °C for 1 h in C_6D_5Br, indicating the strong coordination of THF to the cationic Zr center; the bound THF was not displaced by the added AMA, explaining the inability of this species to polymerize AMA. The polymerization of AMA by **1** was completely shut down when carried out in THF. On the other hand, the discrete complex **3** can be generated by *in situ* mixing of AMA·$B(C_6F_5)_3$ and *rac*-(EBI)ZrMe[$OC(O^iPr)=CMe_2$] in the absence of THF. A kinetic competence check was performed by addition of 10 equiv of AMA to the *in situ*

DOI: 10.1021/jacs.5b05811
J. Am. Chem. Soc. 2015, 137, 9469−9480

Scheme 2. Proposed Mechanism (Propagation Catalysis Cycle) for the Chemoselective and Stereospecific Polymerization of AMA by *rac*-1 As Well As Structures of 1, 3, 3·THF, and 4 As Synthetic Structural Models for Active Species A and Resting-State Chelate B

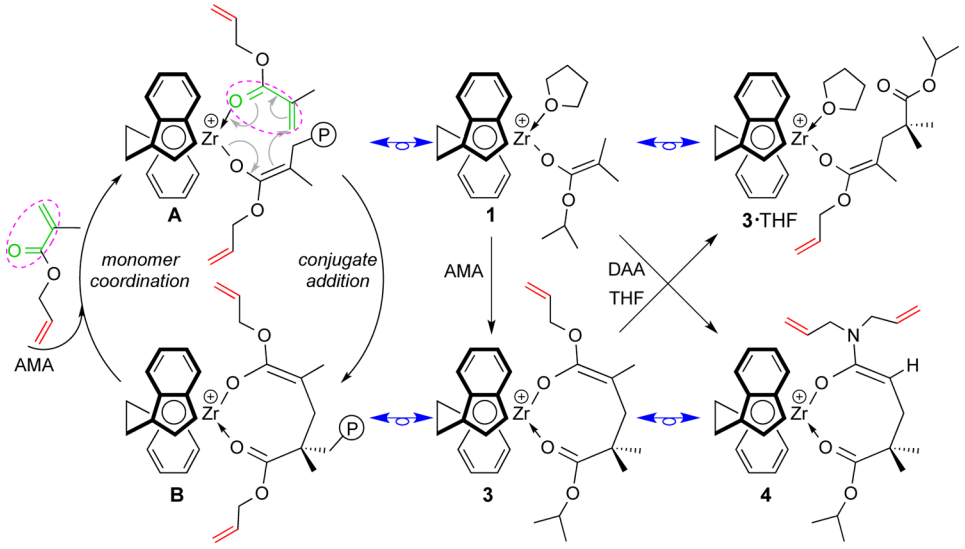

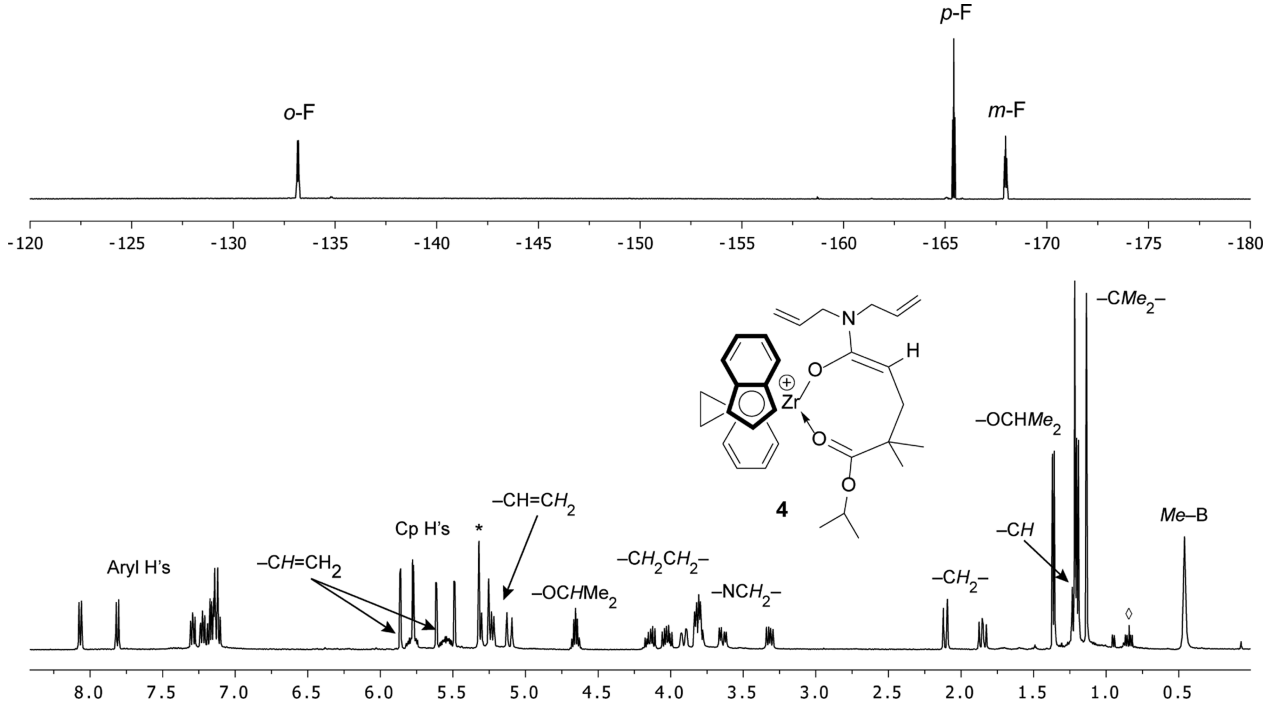

Figure 11. ^{1}H (bottom) and ^{19}F NMR (top) spectra (CD_2Cl_2, 0 °C) of the isolated **4**. Residual NMR and hexanes solvent peaks are labeled as * and ◊, respectively.

generated **3**, which was accompanied by instantaneous formation of *it*-PAMA, thereby confirming the role of **3** as the resting propagating intermediate in the polymerization of AMA by catalyst **1**.

Isolation of the chelating amide enolate intermediate **4** derived from the stoichiometric reaction of **1** and DAA went more smoothly, thanks to its thermal stability and the inability of THF to ring-open the chelate, thus cleanly generating the spectroscopically and analytically pure product **4**. Multinuclear (Figure 11 and Figure S9) and multidimensional (Figures 10 and 11) NMR spectra are consistent with the proposed structure, analogous to the previously isolated eight-membered chelate from the reaction of **1** and *N*,*N*-dimethylacrylamide.[17] Notably, the ^{1}H NMR signal for $-OCHMe_2$ (δ 3.72 ppm, sept) attached to the enolate ligand in **1** is downfield shifted to δ 4.65 ppm for $-OCHMe_2$ now attached to an ester group in **4**, which is consistent with the ^{13}C NMR chemical shift differences for the C(O) carbon: 154.1 ppm for the enolate in **2** [OC(O^{i}Pr)=] and δ 185.0 ppm for the ester in **4** [C(O^{i}Pr)=O]. More importantly, the chemoselective Michael addition of the monomer through the conjugated double bond is confirmed by the presence of the intact $-N(CH_2CH{=}CH_2)_2$ moiety in **4**, as evidenced by (a) ^{1}H NMR: δ 5.79 and 5.55 ppm ($NCH_2CH{=}CH_2$); δ 5.31, 5.24, and 5.11 ppm ($NCH_2CH{=}CH_2$); δ 3.91,

DOI: 10.1021/jacs.5b05811
J. Am. Chem. Soc. 2015, 137, 9469–9480

Scheme 3. Post-Functionalization of *it*-PAMA and *it*-PDAA via the Thiol−Ene Click Chemistry

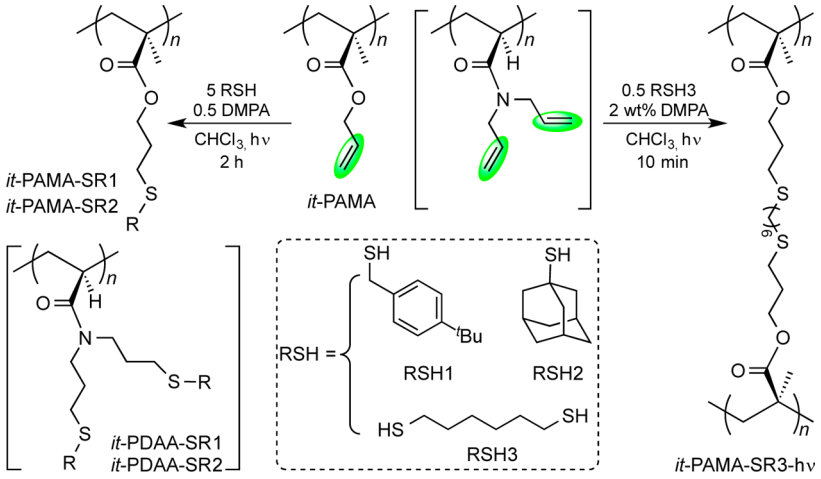

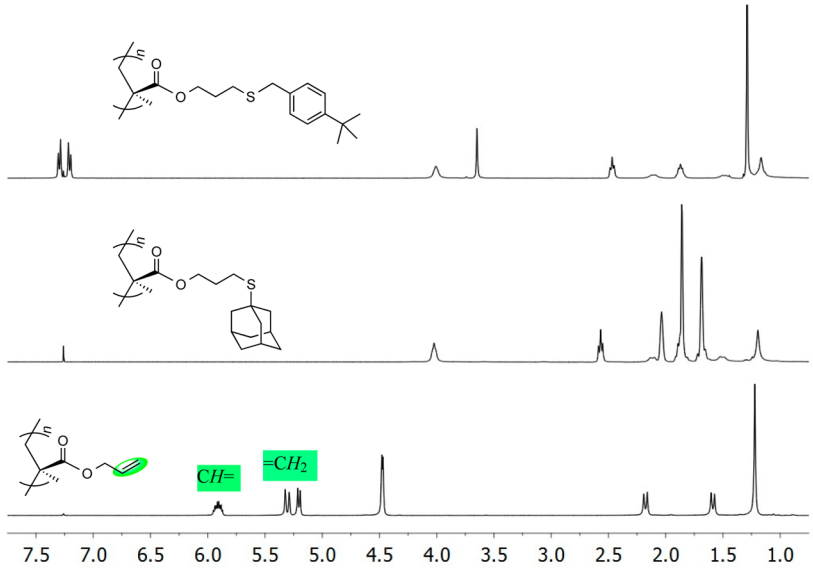

Figure 12. Overlay of ^{1}H NMR ($CDCl_3$, 23 °C) spectra of *it*-PAMA, *it*-PAMA-SR1, and *it*-PAMA-SR2.

3.81, 3.64, and 3.32 ppm ($NCH_2CH{=}CH_2$)], and (b) ^{13}C NMR: δ 132.3 and 131.5 ppm ($NCH_2CH{=}CH_2$); δ 119.7 and 119.0 ppm ($NCH_2CH{=}CH_2$); δ 48.85 and 48.66 ppm ($NCH_2CH{=}CH_2$). The rotation of the allyl amide group around the OC−N bond on the ^{1}H NMR time scale at 25 °C explains the broadening of its signals, but the peaks are markedly sharper at 0 °C. Another advantage of recording the ^{1}H NMR at 0 °C is the assignment of the C*H* signal on the eight-membered ring chelating ligand, which was not detectable at 25 °C due to the overlapping with the broad signals in the olefinic region. At 0 °C the C*H* signal appeared at a much higher field than expected (1.23 ppm), as it was clearly shown by the correlation with the vicinal CH_2 protons in the 2D correlation spectroscopy (Figure S10). Moreover, the 2D HSQC NMR (Figure S11) supports the identification of the corresponding carbon signal in the ^{13}C NMR spectrum, which is also highly upfielded (37.69 ppm, Figure S9). These spectroscopic results suggest that, at lower temperatures, the C*H* moiety in complex **4** could be shielded by the *N*-allyl group (restricted rotation at 0 °C) or complex **4** could be stabilized by a resonance structure where the CH enolate carbon has a more negative charge distribution (i.e., π-allyl type structure). Nevertheless, a kinetic competence check on the isolated chelate **4** revealed that it polymerized 200 equiv of DAA rapidly to produce PDAA with a narrow MW distribution of $Đ$ = 1.17 and a high isotacticity of [*mm*] > 99%, similar to the polymerization started directly with catalyst **1**, thereby confirming the role of the amide enolate **4** as the resting propagating intermediate in the polymerization of DAA by catalyst **1**.

Post-Functionalization to Functional Materials. Post-functionalization of isotactic polymers bearing the pendant vinyl (−CH=CH_2) functional group on every repeating unit was performed through two approaches: the thiol−ene "click" reaction and photocuring. The former approach has been widely used and proven to be highly effective for functionalization of ene-bearing polymers.[18] We first examined functionalization of *it*-PAMA (M_n = 59.8 kg/mol, $Đ$ = 1.25) and *it*-PDAA (M_n = 18.3 kg/mol, $Đ$ = 1.06) with two model thiols, 4-*tert*-butylbenzylmercaptan (RSH1) and 1-adamantanethiol (RSH2), using the click reaction with 2,2-dimethoxy-2-phenylacetophenone (DMPA) as the photoradical initiator under photochemical conditions (RT, UV lamp centered at 350 nm) in chloroform (Scheme 3). The efficiency of this reaction was

DOI: 10.1021/jacs.5b05811
J. Am. Chem. Soc. 2015, 137, 9469−9480

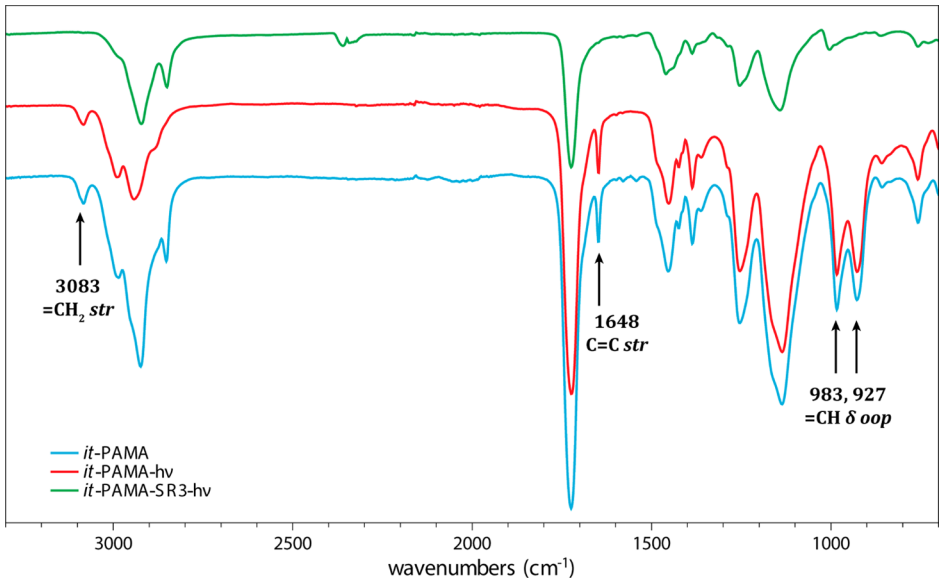

Figure 13. Overlay of IR spectra of *it*-PAMA, *it*-PAMA-*hν*, and *it*-PAMA-SR3-*hν*.

monitored and confirmed by ^{1}H NMR (Figure 12), showing a full conversion of all the pendant double bonds in 2 h; this is evidenced by complete disappearance of the ^{1}H NMR signals corresponding to the olefinic protons in *it*-PAMA (δ 5.91, 5.31, and 5.20 ppm) and *it*-PDAA (δ 5.69 and 5.09 ppm) and appearance of new signals due to the formation of the C−SR bond, observed at δ 2.46 (*it*-PAMA-SR1), 2.57 (*it*-PAMA-SR2), 3.24 (*it*-PDAA-SR1), and 3.60−2.29 ppm (*it*-PDAA-SR2, overlapping with other peaks) for the thioether RSCH_2− protons. The stereochemistry of the resulting thiolated polymers was found to be identical to the parent polymers, with high isotacticity of >95% for *it*-PAMA-SR and >99% for *it*-PDAA-SR in all the cases. However, the thiolated PAMA-SR polymers, which are still soluble in common organic solvents, exhibited much higher MW and $Đ$ values (M_n = 190 kg/mol, $Đ$ = 9.42 for *it*-PAMA-SR1; M_n = 106 kg/mol, $Đ$ = 5.12 for *it*-PAMA-SR2), indicative of some degree of light cross-linking due to the nonselective radical initiation in the presence of the high concentration of reactive C═C pendant groups. On the other hand, *it*-PDAA underwent a much more controlled thiol−ene "click" functionalization, as the MW of the resulting thiolated polymer compares well with the calculated value for both thiolate derivatives, although the $Đ$ values became larger after the thiol−ene reaction: M_n = 36.4 kg/mol (vs the calculated M_n of 36.3 kg/mol) and $Đ$ = 2.68 for *it*-PDAA-SR1; M_n = 36.2 kg/mol (vs the calculated M_n of 35.1 kg/mol), $Đ$ = 2.54 for *it*-PDAA-SR2. Worth noting here is that, when the functionalization was performed using the radical thermoinitiation (i.e., azobis(isobutyronitrile) as the initiator in 1,2-dichlorobenzene, at 70 °C for 24 h), the conversion of all pendant C═C bonds was complete, but the resulting polymer showed a much higher degree of cross-linking with formation of insoluble fractions.

To examine effects of the pendant group functionalization on the polymer thermal properties, the thiol-functionalized polymers were further characterized by thermal gravimetric analysis and DSC, along with their parent polymers. The thiolated *it*-PAMA materials with both 4-*tert*-butylbenzylmercaptan (T_g = 22.1 °C) and 1-adamantanethiol (T_g = 85.5 °C) exhibited a much higher T_g than the parent *it*-PAMA (T_g = 0 °C); the decomposition onset temperature was also substantially enhanced from a T_d of 235 °C of the parent *it*-PAMA to a T_d of 306 and 347 °C of *it*-PAMA-SR1 and *it*-PAMA-SR2, respectively (Figure S4). While the parent *it*-PDAA showed no T_g on its DSC trace, the thiolated analogues *it*-PDAA-SR1 and *it*-PDAA-SR2 revealed a T_g of 42.9 and 146.1 °C, respectively, but a noticeable decrease in T_d from 445 °C of the parent *it*-PDAA to 317 and 405 °C of the thiolated derivatives was observed (Figure S5). It is apparent from the above results that the thiolated isotactic polymers bearing the adamantane group exhibit a much higher T_g and T_d than the polymers carrying the 4-*tert*-butylbenzyl group.

To investigate the photocuring approach, we subjected *it*-PAMA to controlled cross-linking conditions under UV (350 nm) photoradical initiation with DMPA in chloroform inside a Luzchem photoreactor for 10 min. This approach produced an elastic, translucent but colorless thin film (*it*-PAMA-*hν*). The FT-IR spectrum of the film showed the same features as those of the un-cross-linked polymer; of particular interest here are the absorption bands corresponding to the pendant C═C bonds in the cross-linked film [3083 (═CH_2 *str.*); 1648 (C═C *str.*); 983 and 927 (═CH δ *oop*) cm^{-1}], indicating that a significant proportion of olefinic groups did not participate in the photocuring process that yielded the film (Figure 13). The thermal mechanical property of this material was characterized by dynamic mechanical analysis (DMA), and the resulting curves of storage modulus (E'), loss modulus (E''), and tan δ (E''/E') vs temperature are shown in Figure 14. This analysis gave values of E' = 2.674 GPa and E'' = 71.91 MPa at −100 °C or E' = 292.6 MPa and E'' = 199.0 MPa at 25 °C. The T_g of this photocured *it*-PAMA-*hν* obtained from the peak maxima on the tan δ curve is 36.5 °C, which is about 30 °C higher than that of the parent *it*-PAMA. The T_g, if taken as the peak value on the E'' curve, is lower (17.9 °C). When the photocuring of *it*-PAMA was carried out in the presence of 0.5 equiv of a bifunctional thiol (1,6-hexanedithiol, RSH3), a brittle material (*it*-PAMA-SR3-*hν*, Scheme 3) was obtained instead, which was not suitable for DMA analysis in the tension film mode for a comparative study. Interestingly, the analysis of *it*-PAMA-SR3-*hν* by FT-IR revealed no absorption bands attributable to the

DOI: 10.1021/jacs.5b05811
J. Am. Chem. Soc. 2015, 137, 9469−9480

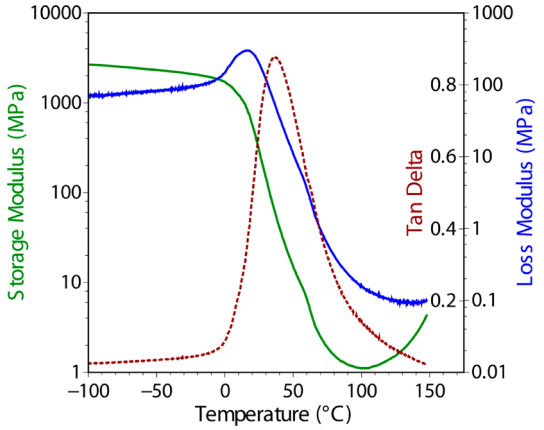

Figure 14. Thermal mechanical spectrum of *it*-PAMA-*hν* obtained by DMA analysis.

olefinic groups (Figure 13), indicating a complete consumption of the pendant C═C bonds. Hence, a combination of photocuring with the thiol−ene "click" reaction in the presence of a photoradical initiator and a dithiol can completely cure the *it*-PAMA carrying the pendant C═C bonds.

CONCLUSIONS

In summary, this work has developed the first chemoselective, stereospecific, and living polymerization of polar divinyl monomers using a chiral *ansa*-zirconocenium ester enolate catalyst. The perfect chemoselectivity is originated from the fact that the polymerization proceeds exclusively through conjugate addition across the methacrylic double bond, which is most activated via coordination of the conjugated carbonyl to the cationic Zr center, while leaving the pendant C═C bonds intact. The stereospecificity is due to an enantiomorphic-site controlled, coordination−addition polymerization mechanism enabled by the chiral *ansa*-zirconocenium ester enolate catalyst, whereas the living nature of the polymerization is brought about by the fast chain initiation through the ester enolate ligand and the lack of problematic chain transfer or termination events, thanks to the chelating resting intermediate involved in the propagation "catalysis" cycle. Key conclusions drawn from our study of the four subareas of the subject are summarized below.

Catalyst Structure. Although only two chiral C_2-ligated *ansa*-zirconocenium ester enolate catalysts have been investigated in this study, the two catalysts have yielded drastically different results. While the newly synthesized and structurally characterized silyl-bridged-*ansa*-zirconocenium ester enolate **2** exhibits low to negligible activity and stereospecificity in the polymerization of the current polar divinyl monomers, the ethylene-bridged-*ansa*-zirconocenium ester enolate **1** is highly active and stereospecific in the polymerization of such monomers. These results showed remarkable sensitivity of the polymerization activity and stereospecificity to a subtle catalyst structure change.

Monomer Structure. The polymerization by catalyst **1** is completely chemoselective for all four representative polar divinyl monomers investigated in this study. The resulting polymers exhibit controlled MW and low $Đ$ values, with the polymerization of DAA showing the highest degree of control over the polymer M_n (nearly identical to the theoretical value) and $Đ$ values (1.06−1.16). The DAA polymerization is also most stereospecific, producing essentially stereoperfect isotactic PDAA with [*mmmm*] > 99%, followed by AMA polymerization, which still led to highly isotactic PAMA with 95−97% [*mm*]. The polymerization of VBMA is further less stereospecific, while the polymerization VMA is least selective. The drastically different stereochemical control over VMA and AMA, where the only structural difference between the two monomers is an additional CH_2 group inserted into the ester oxygen atom and the vinyl carbon in AMA, suggests that the subtle steric difference affects the orientation of the ester OR group and thus its steric interactions with the ligand framework of the catalyst in the transition state determining the stereochemistry of the addition.

Kinetics and Mechanism. We obtained three lines of key evidence from both homo- and block copolymerization experiments to demonstrate living characteristics of the AMA polymerization by **1**. The results of the AMA polymerization kinetics are consistent with the proposed monometallic coordination−addition polymerization mechanism. Synthetic efforts have generated or isolated the first monomer-addition products, **3**, **3**·THF, and **4**, serving as suitable structural models for active species **A** and resting-state chelate **B** (Scheme 2) as well as for performing kinetic competence checks, thus providing additional support for the proposed mechanism.

Post-Functionalization. We employed the thiol−ene "click" reaction and photocuring approaches to post-functionalize isotactic polymers (*it*-PAMA and *it*-PDAA) bearing the pendant vinyl group on every repeating unit. For the thiol−ene reaction, a full conversion of all the pendant double bonds to the corresponding thioether bonds has been achieved for both isotactic polymers, whereas the reaction with *it*-PDAA is more controlled for the MW of the resulting thiolated polymer. The photocuring approach in the presence of a photoradical initiator produced an elastic material readily characterizable by DMA. Performing the photocuring of *it*-PAMA in the presence of 1,6-hexanedithiol produced completely cured *it*-PAMA with all pendant C═C bonds consumed or cross-linked.

ASSOCIATED CONTENT

Supporting Information

Full experimental details and additional figures. The Supporting Information is available free of charge on the ACS Publications website at DOI: 10.1021/jacs.5b05811.

AUTHOR INFORMATION

Corresponding Author

*eugene.chen@colostate.edu

Notes

The authors declare no competing financial interest.

ACKNOWLEDGMENTS

This work was supported by the National Science Foundation (NSF-1300267). We thank Boulder Scientific Co. for the research gift of $B(C_6F_5)_3$.

REFERENCES

(1) Selected reviews: (a) *Stereoselective Polymerization with Single-Site Catalysts*; Baugh, L. S.; Canich, J. A. M., Eds.; CRC Press/Taylor & Francis Group: Boca Raton, FL, 2008. (b) Resconi, L.; Chadwick, J. C.; Cavallo, L. In *Comprehensive Organometallic Chemistry III*; Bochmann, M. Vol. Ed.; Mingos, M. P.; Crabtree, R. H. Chief Eds.; Elsevier: Oxford, 2007; Vol. 4, pp 1005−1166. (c) Coates, G. W. *Chem. Rev.* **2000**, *100*, 1223−1252. (d) Brintzinger, H. H.; Fischer, D.;

DOI: 10.1021/jacs.5b05811
J. Am. Chem. Soc. 2015, 137, 9469−9480

Mülhaupt, R.; Rieger, B.; Waymouth, R. M. *Angew. Chem., Int. Ed. Engl.* **1995**, *34*, 1143−1170.
(2) Selected recent examples and reviews: (a) Jian, Z.; Baier, M. C.; Mecking, S. *J. Am. Chem. Soc.* **2015**, *137*, 2836−2839. (b) Ota, Y.; Ito, S.; Kuroda, J.; Okumura, Y.; Nozaki, K. *J. Am. Chem. Soc.* **2014**, *136*, 11898−11901. (c) Nakamura, A.; Anselment, T. M. J.; Claverie, J. P.; Goodall, B.; Jordan, R. F.; Mecking, S.; Rieger, B.; Sen, A.; van Leeuwen, P. W. N. M.; Nozaki, K. *Acc. Chem. Res.* **2013**, *46*, 1438−1449. (d) Delferro, M.; Marks, T. J. *Chem. Rev.* **2011**, *111*, 2450−2485. (e) Nakamura, A.; Ito, S.; Nozaki, K. *Chem. Rev.* **2009**, *109*, 5215−5244. (f) Berkefeld, A.; Mecking, S. *Angew. Chem., Int. Ed.* **2008**, *47*, 2538−2542. (g) Luo, S.; Vela, J.; Lief, G. R.; Jordan, R. F. *J. Am. Chem. Soc.* **2007**, *129*, 8946−8947. (h) Domski, G. J.; Rose, J. M.; Coates, G. W.; Bolig, A. D.; Brookhart, M. *Prog. Polym. Sci.* **2007**, *32*, 30−92. (i) Jensen, T. R.; Yoon, S. C.; Dash, A. K.; Luo, L.; Marks, T. J. *J. Am. Chem. Soc.* **2003**, *125*, 14482−14494. (j) Gibson, V. C.; Spitzmesser, S. K. *Chem. Rev.* **2003**, *103*, 283−315. (k) Coates, G. W.; Hustad, P. D.; Reinartz, S. *Angew. Chem., Int. Ed.* **2002**, *41*, 2236−2257. (l) Ittel, S. D.; Johnson, L. K.; Brookhart, M. *Chem. Rev.* **2000**, *100*, 1169−1204.
(3) Selected examples and reviews: (a) Zhang, N.; Salzinger, S.; Soller, B. S.; Rieger, B. *J. Am. Chem. Soc.* **2013**, *135*, 8810−8813. (b) Chen, E. Y.-X. *Chem. Rev.* **2009**, *109*, 5157−5214. (c) Lian, B.; Spanio, T. P.; Okuda, J. *Organometallics* **2007**, *26*, 6653−6660. (d) Lian, B.; Thomas, C. M.; Navarro, C.; Carpentier, J.-F. *Organometallics* **2007**, *26*, 187−195. (e) Stojcevic, G.; Kim, H.; Taylor, N. J.; Marder, T. B.; Collins, S. *Angew. Chem., Int. Ed.* **2004**, *43*, 5523−5526. (f) Strauch, J. W.; Fauré, J.-L.; Bredeau, S.; Wang, C.; Kehr, G.; Fröhlich, R.; Luftmann, H.; Erker, G. *J. Am. Chem. Soc.* **2004**, *126*, 2089−2104. (g) Frauenrath, H.; Keul, H.; Höcker, H. *Macromolecules* **2001**, *34*, 14−19. (h) Bandermann, F.; Ferenz, M.; Sustmann, R.; Sicking, W. *Macromol. Symp.* **2001**, *174*, 247−253. (i) Yasuda, H. *Prog. Polym. Sci.* **2000**, *25*, 573−626. (j) Cameron, P. A.; Gibson, V.; Graham, A. J. *Macromolecules* **2000**, *33*, 4329−4335. (k) Li, Y.; Ward, D. G.; Reddy, S. S.; Collins, S. *Macromolecules* **1997**, *30*, 1875−1883. (l) Deng, H.; Shiono, T.; Soga, K. *Macromolecules* **1995**, *28*, 3067−3073. (m) Collins, S.; Ward, S. G. *J. Am. Chem. Soc.* **1992**, *114*, 5460−5462. (n) Yasuda, H.; Yamamoto, H.; Yokota, K.; Miyake, S.; Nakamura, A. *J. Am. Chem. Soc.* **1992**, *114*, 4908−4909.
(4) (a) He, J.; Zhang, Y.; Chen, E. Y.-X. *Macromol. Symp.* **2015**, *349*, 104−114. (b) Zhang, Y.; Caporaso, L.; Cavallo, L.; Chen, E. Y.-X. *J. Am. Chem. Soc.* **2011**, *133*, 1572−1588.
(5) (a) Gao, H.; Matyjaszewski, K. *Prog. Polym. Sci.* **2009**, *34*, 317−350. (b) Li, Z.; Day, M.; Ding, J.; Faid, K. *Macromolecules* **2005**, *38*, 2620−2625. (c) Percec, V.; Auman, B. C. *Makromol. Chem.* **1984**, *185*, 2319−2336.
(6) (a) Ma, J.; Cheng, C.; Sun, G. R.; Wooley, K. L. *Macromolecules* **2008**, *41*, 9080−9089. (b) París, R.; de la Fuente, J. L. *J. Polym. Sci., Part A: Polym. Chem.* **2005**, *43*, 6247−6261. (c) París, R.; de la Fuente, J. L. *J. Polym. Sci., Part A: Polym. Chem.* **2005**, *43*, 2395−2406. (d) Nagelsdiek, R.; Mennicken, M.; Maier, B.; Keul, H.; Höcker, H. *Macromolecules* **2004**, *37*, 8923−8932.
(7) Vardareli, T. K.; Keskin, S.; Usanmaz, A. *J. Macromol. Sci., Part A: Pure Appl.Chem.* **2008**, *45*, 302−311.
(8) Sugiyama, F.; Satoh, K.; Kamigaito, M. *Macromolecules* **2008**, *41*, 3042−3048.
(9) (a) Lu, Z.; Lee, S. Y.; Goh, S. H. *Polymer* **1997**, *38*, 5893−5895. (b) Fukuda, W.; Nakao, M.; Okumura, K.; Kakiuchi, H. *J. Polym. Sci., Part A-1: Polym. Chem.* **1972**, *10*, 237−250.
(10) Jia, Y.-B.; Ren, W.-M.; Liu, S.-J.; Xu, T.; Wang, Y.-B.; Lu, X.-B. *ACS Macro Lett.* **2014**, *3*, 896−899.
(11) Pugh, C.; Percec, V. *Polym. Bull.* **1985**, *14*, 109−116.
(12) Murali Mohan, Y.; Raghunadh, V.; Sivaram, S.; Baskaran, D. *Macromolecules* **2012**, *45*, 3387−3393.
(13) Chen, E. Y. *Top. Curr. Chem.* **2013**, *334*, 239−260.
(14) Chen, J.; Chen, E. Y.-X. *Isr. J. Chem.* **2015**, *55*, 216−225.
(15) Bolig, A. D.; Chen, E. Y.-X. *J. Am. Chem. Soc.* **2004**, *126*, 4897−4906.
(16) Rodriguez-Delgado, A.; Chen, E. Y.-X *Macromolecules* **2005**, *38*, 2587−2594.
(17) (a) Mariott, W. R.; Chen, E. Y.-X. *Macromolecules* **2005**, *38*, 6822−6832. (b) Mariott, W. R.; Chen, E. Y.-X. *Macromolecules* **2004**, *37*, 4741−4743.
(18) For selected reviews, see: (a) Barner-Kowollik, C.; Du Prez, F. E.; Espeel, P.; Hawker, C. J.; Junkers, T.; Schlaad, H.; Van Camp, W. *Angew. Chem., Int. Ed.* **2011**, *50*, 60−62. (b) Hoyle, C. E.; Bowman, C. N. *Angew. Chem., Int. Ed.* **2010**, *49*, 1540−1573. (c) Iha, R. K.; Wooley, K. L.; Nyström, A. M.; Burke, D. J.; Kade, M. J.; Hawker, C. J. *Chem. Rev.* **2009**, *109*, 5620−5686. (d) Binder, W. H.; Sachsenhofer, R. *Macromol. Rapid Commun.* **2008**, *29*, 952−981. (e) Binder, W. H.; Sachsenhofer, R. *Macromol. Rapid Commun.* **2007**, *28*, 15−54.
(19) Chen, X.; Caporaso, L.; Cavallo, L.; Chen, E. Y.-X. *J. Am. Chem. Soc.* **2012**, *134*, 7278−7281.
(20) (a) Miyake, G. M.; Chen, E. Y.-X. *Macromolecules* **2008**, *41*, 3405−3416. (b) Miyake, G. M.; Mariott, W. R.; Chen, E. Y.-X. *J. Am. Chem. Soc.* **2007**, *129*, 6724−6725.
(21) (a) Stehling, U.; Diebold, J.; Kirsten, R.; Roell, W.; Brintzinger, H.-H.; Juengling, S.; Muelhaupt, R.; Langhauser, F. *Organometallics* **1994**, *13*, 964−970. (b) Spaleck, W.; Kueber, F.; Winter, A.; Rohrmann, J.; Bachmann, B.; Antberg, M.; Dolle, V.; Paulus, E. F. *Organometallics* **1994**, *13*, 954−963.
(22) Bolig, A. D.; Chen, E. Y.-X. *J. Am. Chem. Soc.* **2002**, *124*, 5612−5613.
(23) Mariott, W. R.; Rodriguez-Delgado, A.; Chen, E. Y.-X. *Macromolecules* **2006**, *39*, 1318−1327.
(24) Diamond, G. M.; Jordan, R. F.; Petersen, J. L. *J. Am. Chem. Soc.* **1996**, *118*, 8024−8033.
(25) Klosin, J.; Roof, G. R.; Chen, E. Y.-X.; Abboud, K. A. *Organometallics* **2000**, *19*, 4684−4686.
(26) Horton, A. D.; de With, J.; van der Linden, A. J.; van de Weg, H. *Organometallics* **1996**, *15*, 2672−2674.
(27) Yang, X.; Stern, C. L.; Marks, T. J. *J. Am. Chem. Soc.* **1991**, *113*, 3623−3625.
(28) (a) Caporaso, L.; Cavallo, L. *Macromolecules* **2008**, *41*, 3439−3445. (b) Caporaso, L.; Gracia-Budrìa, J.; Cavallo, L. *J. Am. Chem. Soc.* **2006**, *128*, 16649−16654.
(29) Greenley, R. Z. In *Polymer Handbook*, 3rd ed.; Immergut, E. H., Brandup, J., Eds.; Wiley: New York, 1989; pp 267−274.

DOI: 10.1021/jacs.5b05811
J. Am. Chem. Soc. 2015, 137, 9469−9480